

1 Simultaneous Measurement of Urban and Rural Single Particles in Beijing, Part I:
2 Chemical Composition and Mixing State

3 Yang Chen¹, Jing Cai², Zhichao Wang¹, Chao Peng¹, Xiaojiang Yao¹, Mi Tian¹, Yiqun
4 Han², Guangming Shi^{1,3}, Zongbo Shi⁴, Yue Liu², Xi Yang², Mei Zheng^{2*}, Tong Zhu², Kebin
5 He⁵, Qiang Zhang⁶, and Fumo Yang^{3,1*}

6 ¹Center for the Atmospheric Environment Research, Chongqing Institute of Green and
7 Intelligent Technology, Chinese Academy of Sciences, Chongqing 400714, China

8 ²SKL-ESPC and BIC-ESAT, College of Environmental Sciences and Engineering, Peking
9 University, Beijing 100871, China

10 ³College of Architecture and Environment, Sichuan University, Chengdu 610065, China

11 ⁴ School of Geography Earth and Environmental Sciences, University of Birmingham,
12 Birmingham B15 2TT, UK

13 ⁵ School of Environment, Tsinghua University, Beijing 100084, China

14 ⁶Department of Earth System Science, Tsinghua University, Beijing, China

15 Corresponding to Fumo Yang (fmyang@scu.edu.cn) and Mei Zheng
16 (mzheng@pku.edu.cn)

17 Keywords: urban; regional; single particle; transport; mixing state

18 **Abstract**

19 Two single particle aerosol mass spectrometers (SPAMS) were deployed simultaneously
20 at an urban and a rural site in Beijing during an intensive field campaign from 1st to 29th
21 Nov 2016 to investigate the source and process of airborne particles in Beijing. In the first
22 part of this research, we report the single-particle chemical composition, mixing state, and
23 evolution at both sites. 96% and 98% of collected particles were carbonaceous at the urban
24 and rural sites, respectively. Five particle categories, including elemental carbon (EC),
25 organic carbon (OC), internal-mixed EC and OC (ECOC), potassium-rich (K-rich), and
26 Metals were observed at both sites. The categories were partitioned into particle types
27 depending on different atmospheric processing stages. Seventeen particle types were
28 shared at both sites. In the urban area, nitrate-containing particle types, such as EC-Nit and
29 ECOC-Nit, were enriched, especially at night; sulfate-containing particles were transported
30 when wind speed was high; ECOC-Nit-Sul were mostly local-aged. In sum, these
31 processed particles took up to 85.3% in the urban areas. In the rural area, regional particles
32 were abundant, but freshly emitted ECOC and OC had distinct patterns that were
33 pronounced at cooking and heating time. Biomass burning, traffic, and coal burning were
34 major sources of PM_{2.5} in both rural and urban areas. Besides, the particles from the steel
35 industry located in the south were also identified. In summary, the chemical composition
36 of urban and rural particle types was similar in Beijing; the urban particles were influenced
37 significantly by rural processing and transport. The work is useful to understand the
38 evolution of urban and rural particles in Beijing during winter.

39 **1. Introduction**

40 China has experienced severe haze events caused by extremely high concentrations of fine
41 particulate matter (PM_{2.5}) since January 2013. In the worst cases, an area of 2.0 million
42 km² and a population of 800 million were affected (Huang et al., 2014). In the Beijing-
43 Tianjin-Hebei (BTH) area, extreme haze events frequently occur during winter, with PM_{2.5}
44 mass reaching rapidly up to 200 μg m⁻³ and sustaining such levels for hours (Guo et al.,
45 2014).

46 Over the last two decades, comprehensive studies have been conducted on urban PM in
47 Beijing. He et al. (2001) reported the first characterization of PM_{2.5}. Since then, numerous
48 studies have been published on characterization (Huang et al., 2010), sources (Guo et al.,
49 2012; Sun et al., 2014a), and processing of PM (Sun et al., 2013). The mechanism of rapid-
50 boosting PM_{2.5} in Beijing, including new particle formation and growth (Guo et al., 2014),
51 regional transport (Li et al., 2015a), and both (Du et al., 2017; Sun et al., 2014a), have been
52 proposed. However, discrepancies remain among these studies. For example, the mass
53 loading of PM_{2.5} can rapidly increase to hundreds of μg m⁻³. Both Wang et al. (2016b) and
54 Cheng et al. (2016) suggested the secondary formation of sulfate from the oxidation of
55 NO₂; while (Guo et al., 2014) have proposed a mechanism of particle formation and growth.
56 Different from local secondary formation and accumulation, Li et al. (2015b) proposed that
57 particles via long-range transport cause the elevation of PM_{2.5}. According to Sun et al.
58 (2014b) and Zhai et al. (2016), regional transport played important roles during heavy haze
59 episodes. However, most of the studies have focused on the urban areas of Beijing, with

60 limited attention to the rural areas. To illustrate the sources, evolution, and transport of
61 particles. The investigation of rural areas around Beijing is necessary.”

62 Single particle mass spectrometers (SPMS) have been used to investigate the size-resolved
63 chemical composition and mixing state of atmospheric particles (Gard et al., 1997; Pratt
64 and Prather, 2012). More recently, single particle aerosol mass spectrometers (SPAMS)
65 have been used in Chinese megacities such as Beijing (Li et al., 2014), Shanghai (Tao et
66 al., 2011), Guangzhou (Bi et al., 2011), Xi’an (Chen et al., 2016), Nanjing (Wang et al.,
67 2015), and Chongqing (Chen et al., 2017). SPAMS has been proven a useful tool for
68 characterizing the single-particle chemical composition, mixing state, and processing of
69 atmospheric particles. Due to the nature of laser desorption/ionization (LDI), the
70 instrument is very sensitive to dust or other types of particles containing sodium and
71 potassium. This may cause bias on the particle matrix (Pratt and Prather, 2012).

72 In Beijing, particle types, such as carbonaceous, metal, dust, K-rich, and others during
73 spring and fall, were reported (Liu et al., 2016b; Li et al., 2014). Besides, lead-containing
74 particles have also been investigated in recent studies (Ma et al., 2016; Cai et al., 2017).
75 Organics, sulfate, nitrate, ammonium, and other species have been found internally mixed
76 in the atmospheric particles, and these particle types are mostly from combustion of fuel
77 or biomass. The abundance of secondary species can indicate the degree of aging during
78 atmospheric processing. Particles are more secondary species with deeper processing.
79 However, these studies are lack of using these data to provide a view of dynamic particulate
80 processing. These studies have focused on the urban areas of Beijing, causing limited

81 information to characterize the particles in the Beijing Region. Therefore, a simultaneous
82 study to investigate the particle chemical composition and mixing state would fill the gap.

83 This study is a part of the APHH-Beijing (Atmospheric Pollution and Human Health in a
84 Chinese Megacity of Beijing) intensive field campaign during winter 2016 (Shi et al., 2019).
85 Two SPAMSs were deployed simultaneously at Peking University (PKU) and Pinggu (PG)
86 in order to observe both urban and rural particles in the Beijing region. The aims of the
87 study are 1) to characterize the single-particle chemical composition and mixing state; 2)
88 to investigate particulate evolution at both sites during haze events. These two objectives
89 are presented in two parts. In Part I, particle types and their atmospheric processing (e.g.,
90 origination, source, and diurnal profiles) at both sites are reported; in Part II, the detailed
91 analysis of haze events, effects of heating activities, and evidence of regional transport are
92 addressed.

93 **2. Methodology**

94 **2.1 Sampling sites**

95 The campaigns were performed simultaneously at PKU (116.32°E, 39.99°N) and PG
96 (117.05°E, 40.17°N) from 11/01/2016 to 11/29/2016. A Description of the PKU site is
97 available in the literature (Huang et al., 2006). Briefly, the site is located on the rooftop (15
98 m above the ground) on the PKU campus which is surrounded by residential and
99 commercial blocks. Trace gases (Thermo Inc. series), meteorological parameters (Vaisala
100 Inc.), and PM_{2.5} (TEOM 1430) were recorded during the observation.

101 The PG site (117.053°E, 40.173°N) is 3 km from the PG center. The site is located in the
102 northeast of the PKU site with a distance of 70 km. The PG site also acts as a host of the
103 AIRLESS (Effects of AIR pollution on the cardiopulmonary disease in urban and peri-
104 urban residents in Beijing) Project. The meteorological data is acquired from the local
105 meteorological office. The PG village is surrounded by orchards and farmland with no
106 main road nearby on a scale of 3 km. Coal and biomass are used for domestic heating and
107 cooking in the nearby villages.

108 **2.2 Instrumentation and data analysis**

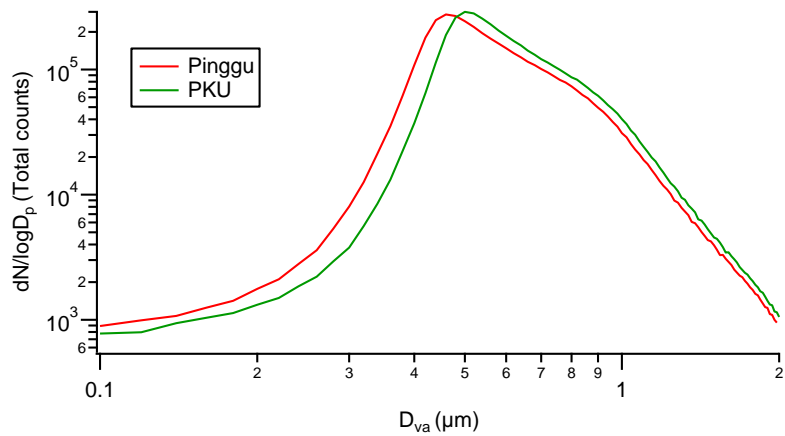
109 Two SPAMSs (Model 0515, Hexin Inc., Guangzhou, China) were deployed at both PKU
110 and PG. A technical description of SPAMS is available in (Li et al., 2011). Briefly, a
111 SPAMS has three functional parts: sampling, sizing, and mass spectrometry. In the
112 sampling part, particles within a 0.1–2.0 μm size range pass efficiently through an
113 aerodynamic lens. In the sizing unit, the aerodynamic diameter (D_{va}) is calculated using
114 the time-of-flight of particles. The particles are then decomposed and ionized into ions one-
115 by-one using a 266 nm laser. A bipolar time-of-flight mass spectrometer measures the ions
116 and generates the positive and negative mass spectra of each particle. The two instruments
117 were maintained and calibrated following the standard procedures before sampling (Chen
118 et al., 2017).

119 A neural network algorithm based on adaptive resonance theory (ART-2a) was used to
120 resolve particle types from both datasets (Song et al., 1999). The parameters used were: a
121 vigilance factor of 0.70, a learning rate of 0.05, and 20 iterations. This procedure generated
122 771 and 792 particle groups. Then, the groups were combined into particle types based on

123 similar mass spectra, temporal trends, and size distributions (Dallosto and Harrison, 2006).
124 During combining, relative areas of nitrate and sulfate were used to distinguish the stages
125 of processing, assuming that more sulfate and nitrate can be measured if a particle is more
126 processed during its lifetime. Thus, particles with relative peak areas of sulfate and nitrate
127 larger than 0.1 were marked with nitrate (-Nit), sulfate (-Sul), respectively, or both. Indeed,
128 matrix effect can affect ionic intensities between different particles during single-particle
129 mass spectrometer analysis. However, the effect can be reduced using average mass spectra
130 of particles within the similar size distribution and chemical composition. Finally, the
131 strategy resulted in 20 and 19 particle types at PKU and PG respectively. Among them, 17
132 types appeared at both sites, and each type has identical mass spectra ($R^2 > 0.80$) between
133 each other.

134 **3. Results**

135 A total of 4,499,606 and 4,063,522 particles were collected at PKU and PG sites,
136 respectively. The size distributions peaked at 0.48 μm and 0.52 μm (Figure 1). The smaller
137 size distribution was due to a more substantial fraction of freshly-emitted particles at PG,
138 as described in Table 1. Seventeen particle types ($R^2 > 0.80$, mass spectra) were observed
139 both at PKU and PG (Table 1). These particle types were labeled with the suffixes “_PKU”
140 or “_PG” to indicate their locations. The term “particle category” stands for a group of
141 particle types with variable stages of processing.



142

143 Figure 1. The size distribution of SPAMS particles at PKU and PG sites.

144

145 Table 1. SPAMS particle types identified at PKU and PG sites.

Particle type	PKU	PKU	PG	PG	Comments
	Number	Percentage	Number	Percentage	
EC-Nit	313574	7.0	79082	2.0	Solid fuel burning, traffic
EC-Nit-Sul	473908	10.5	140107	3.5	
EC-Sul	30365	0.7	4096	0.1	
ECOC-Nit-Sul	539533	12.0	755279	18.6	Traffic, coal burning
ECOC-Sul	572548	12.7	397367	9.8	
K-rich	322731	7.2	259287	6.4	Aged biomass burning
K-Nit	359281	8.0	334547	8.2	
K-Nit-Sul	717280	16.0	76954	1.9	
K-Sul	26301	0.6	183571	4.5	
NaK	16680	0.4	74943	1.8	Coal, peat
NaK-Nit	289259	6.4	69760	1.7	
NaK-Nit-Sul	114387	2.5	77555	1.9	
NaK-Sul	7509	0.2	16578	0.4	
OC-Nit-Sul	334870	7.4	865821	21.3	Traffic, coal burning
OC-Sul	40800	0.9	279322	6.9	
Ca-dust	19869	0.4	3035	0.1	dust
Fe-rich	137600	3.1	70920	1.8	Steel industry
ECOC-Nit	137470	3.1%			Solid fuel burning
OC-Nit	41159	0.9%			Traffic, coal burning
K-Amine-Nit-Sul	4482	0.1%			Coal burning
ECOC			239953	5.9%	Coal burning
OC			135345	3.3%	Traffic, coal burning

146

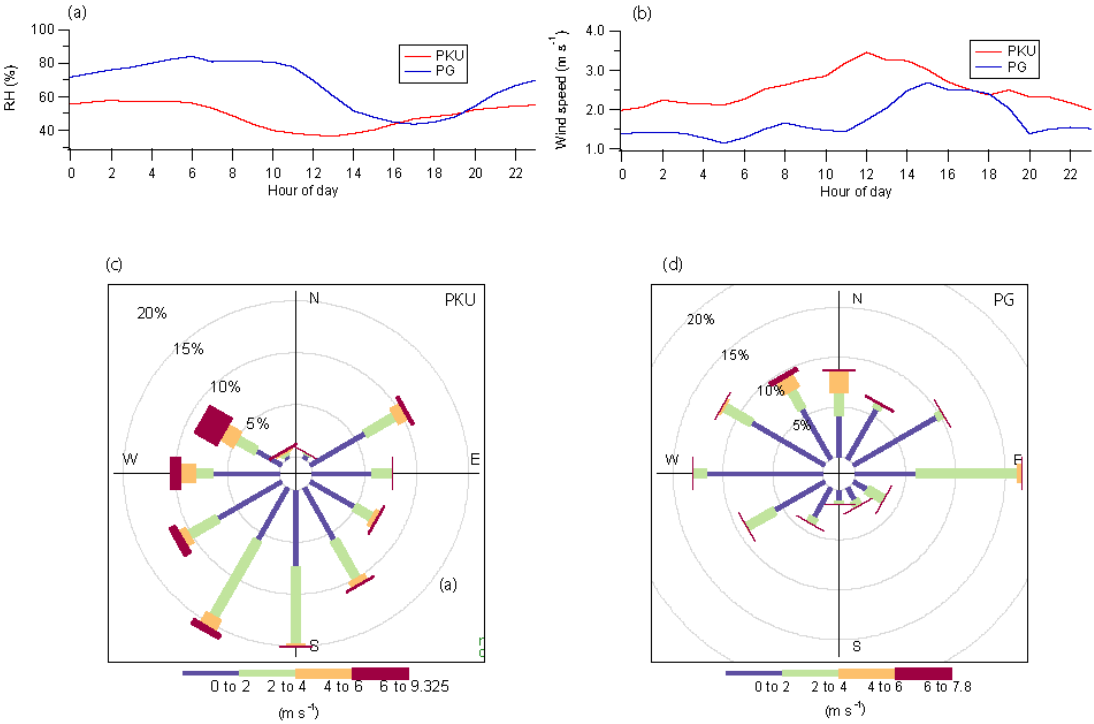
147 Note: Nit stands for nitrate, Sul for sulfate.

148 **3.1 Meteorological conditions and overview**

149 Temperature, relative humidity (RH), and wind speed at both sites during the sampling
 150 period are summarized in Table 2. Their temporal trends are available in Part II. The

151 average temperature at PKU (urban, 5.7 ± 2.3 °C) was higher than at PG (rural, 3.1 ± 2.2 °C).
 152 Correspondingly, relative humidity was higher at PG ($67\pm 32\%$) than at PKU ($49\pm 30\%$).
 153 The wind was stronger at PKU (2.5 ± 1.8 ms⁻¹) than at PG (1.7 ± 0.9 ms⁻¹). As shown in
 154 Figure 2, at PKU, wind speed peaked at noon (local time, UTC+8), while at PG, wind speed
 155 reached its maxima at 15:00. Various wind speeds determined the different dispersion
 156 patterns of pollutants near the surface. It should be noticed that wind speed up to 2 ms⁻¹
 157 representing a scale of 172 km in diurnal transport. Therefore, at PKU, the wind could
 158 bring the pollutants from Hebei province under stagnant air conditions.

159



160

161 Figure 2. Diurnal plots of (a) RH and (b) wind speed, and rose plots of wind at (c)PKU and
 162 (d) PG.

163 Table 2. Meteorological parameters at PKU and PG during the campaign.

	PKU	PG
Temperature (°C)	5.7±2.3	3.1±2.2
RH (%)	49±30	67±32
Wind speed (ms ⁻¹)	2.5± 1.8	1.7± 0.9

164

165 **3.2 Common particle categories at both PKU and PG**

166 **3.2.1 Elemental carbon (EC)**

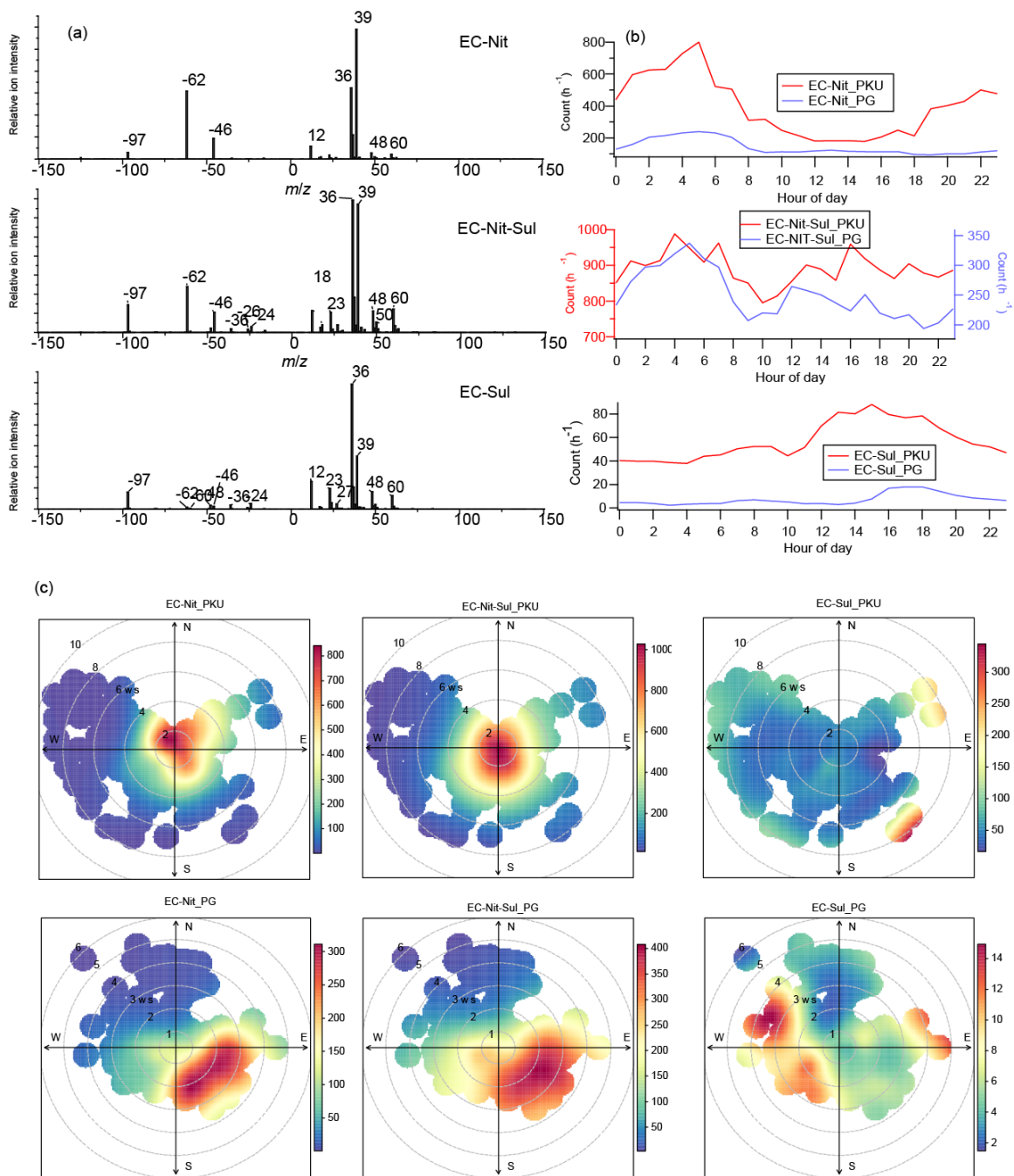
167 As shown in Figure 3a, the elemental carbon (EC) particle category was represented by
 168 ions peaking at m/z 12, 24, 36, 48, and 60 in positive mass spectra (Sodeman et al., 2005;
 169 Toner et al., 2008). EC is emitted from solid fuel combustion, traffic (Sodeman et al., 2005;
 170 Toner et al., 2008; Toner et al., 2006), and industrial activities (Healy et al., 2012). Due to
 171 the various ionic intensities of nitrate (m/z -46 and -62) and sulfate (m/z -80 and -97), the
 172 EC category has four types including EC-Nitrate (EC-Nit), EC-Sulfate (EC-Sul), and EC-
 173 Nit-Sul. Besides, the EC category was more abundant after the heating began rather than
 174 before (Part II), indicating that coal burning was one of the primary sources.

175 EC-Nit_PKU and EC-Nit_PG accounted for 7.0% and 2.0% in PKU and PG datasets,
 176 respectively. In the diurnal profiles of EC-Nit_PKU, there was an apparent early morning
 177 peak at 5:00 (UTC+8, local time), along with an evening peak (22:00). There was also an
 178 early morning NO_x peak in the urban area of Beijing, providing sufficient precursors for
 179 secondary nitrate (Shi et al., 2019). Wang et al. (2018) validated the role of N₂O₅ uptake
 180 on the nitrate formation in PM. Therefore, the early morning peak of EC-Nit_PKU
 181 occurred due to the uptake of nitrate on the freshly emitted EC in the early morning (Sun
 182 et al., 2014a). The evening peak could be due to the low temperature after the heating

183 supply started (Liu et al., 2019a). Diurnally, EC-Nit_PG exhibited an early morning peak
184 (5:00) but no evening peak and mainly came from the southeast.

185 EC-Nit-Sul was more abundant at the rural site (18.6%) than the urban site (11.6%). EC-
186 Nit-Sul_PKU (10.5%) had early morning (04:00), morning (7:00), and afternoon peaks
187 (around 16:00), while EC-Nit-Sul_PG (3.5%) had early morning (04:00), noon, and
188 afternoon peaks (17:00, Figure 3a). However, they showed relatively small diurnal
189 variations. For example, EC-Nit-Sul_PKU varied between 800 h^{-1} and $1,000 \text{ count h}^{-1}$, and
190 EC-Nit-Sul_PG shifted between 200 count h^{-1} and 250 count h^{-1} . Thus, the EC-Nit-Sul at
191 both sites was most likely acting as background and regional particles (Dall'Osto et al.,
192 2016). Additionally, EC-Nit-Sul_PKU mainly came from the surrounding area in the city
193 pollutant plume, while EC-Nit-Sul_PG mainly came from the southeast (Figure 3c).

194 EC-Sul was a minor type at both sites, accounting for 0.7% at PKU and 0.1% at PG. EC-
195 Sul was pronounced in the afternoon when the wind was strong at both sites. It was unlikely
196 for either EC-Sul_PKU or EC-Sul_PG to be local because their concentrations were
197 associated with high wind speed, as shown in Figure 3c. More specifically, EC-Sul_PKU
198 came from the southeast and northeast of Hebei Province when the wind speed exceeded
199 6 m s^{-1} . EC-Sul_PG could come from the west when the wind speed exceeded 2 m s^{-1} and
200 the east when the wind speed exceeded 3 m s^{-1} , as coal-using industries are located in both
201 directions. Also, at both sites, the concentrations of SO_2 were elevated in the afternoon due
202 to transport, providing sufficient precursors for the formation of sulfate (Shi et al., 2019).



203

204 Figure 3. (a) average mass spectra of EC-Nit, EC-Nit-Sul, and EC-Sul at both sites; (b)
 205 diurnal patterns of EC-Nit, EC-Nit-Sul, and EC-Sul at both sites; (c) polar plots of EC-Nit,
 206 EC-Nit-Sul, and EC-Sul; the grey circles indicate wind speed (m s^{-1}).

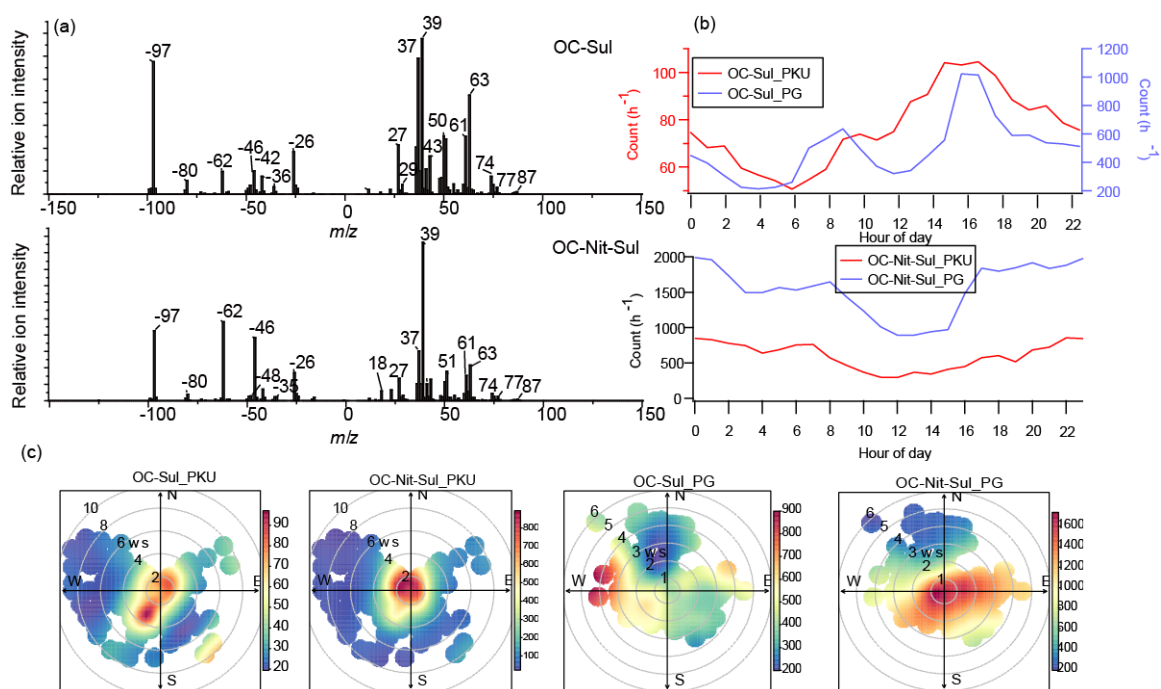
207 3.2.2 Organic carbon (OC) category

208 The positive mass spectra of both OC-Nit and OC-Nit-Sul contained complicated organic
209 ions such as $C_2H_3^+$ (m/z 27), C_3H^+ (m/z 37), $C_3H_7^+/C_2H_3O^+/CHNO^+$ (m/z 43), $C_4H_2^+$ (m/z
210 50), aromatic hydrocarbons ($C_4H_3^+$, $C_5H_3^+$, and $C_6H_5^+$), and diethylamine ($(C_2H_5)_2NH_2^+$,
211 m/z 74), $(C_2H_5)_2NCH_2^+$ (m/z 86)). The negative mass spectra contained CN^- (m/z -26), Cl^-
212 (m/z -35 and 37), CNO^- (m/z -42), nitrate (m/z -46 and -62), and sulfate (m/z -97). The
213 presence of CN^- and CNO^- suggests the existence of organonitrogen species (Day et al.,
214 2010). Peak intensities of organic fragments are relatively high in the OC-Sul particles,
215 indicating that it was relatively fresh, while OC-Nit-Sul was more processed (Zhai et al.,
216 2015; Peng et al., 2020a). The positive mass spectrum had similar ions of Coal Combustion
217 OA (CCOA) with significant signals of PAHs in AMS studies (Sun et al., 2013). OC-Sul
218 showed different spatial distributions with 0.9% at PKU and 6.9% at PG.

219 OC-Sul_PG had morning (8:00) and afternoon (16:00) peaks, while the diurnal profile of
220 OC-Sul_PKU showed a trend with an early morning (3:00), morning (10:00), and
221 afternoon peaks (16:00). The diurnal trends OC-Sul at both PKU and PG were consistent
222 with the heating pattern depending on the variation of local temperature. Moreover, OC-
223 Sul_PG increased after the heating supply began. Polar plots suggest that OC-Sul_PKU
224 came from surrounding southwest areas via transport, while OC-Sul_PG came from
225 villages to the east and west (Figure 4). These results suggest that OC-Sul_PG was emitted
226 from coal burning for residential heating in nearby areas.

227 OC-Nit-Sul accounted for 7.4 % and 21.3 % of all detected particles at PKU and PG,
228 respectively. OC-Nit-Sul_PKU had a diurnal peak at 7:00 in rush hours, suggesting that

229 OC-Nit-Sul could be formed due to the uptake of nitrate on OC-Sul. While OC-Nit-Sul_PG
 230 had a diurnal peak at 8:00 due to traffic in nearby towns. As an aged particle type, OC-Nit-
 231 Sul_PKU and OC-Nit-Sul_PG, also acting as a similar type of background types with
 232 hourly counts remained low but elevated to high levels at night. Polar plots suggest that
 233 OC-Nit-Sul_PKU mainly came from the surrounding areas, while OC-Nit-Sul_PG mainly
 234 came from the south and east, where populous villages are located (Figure 4).

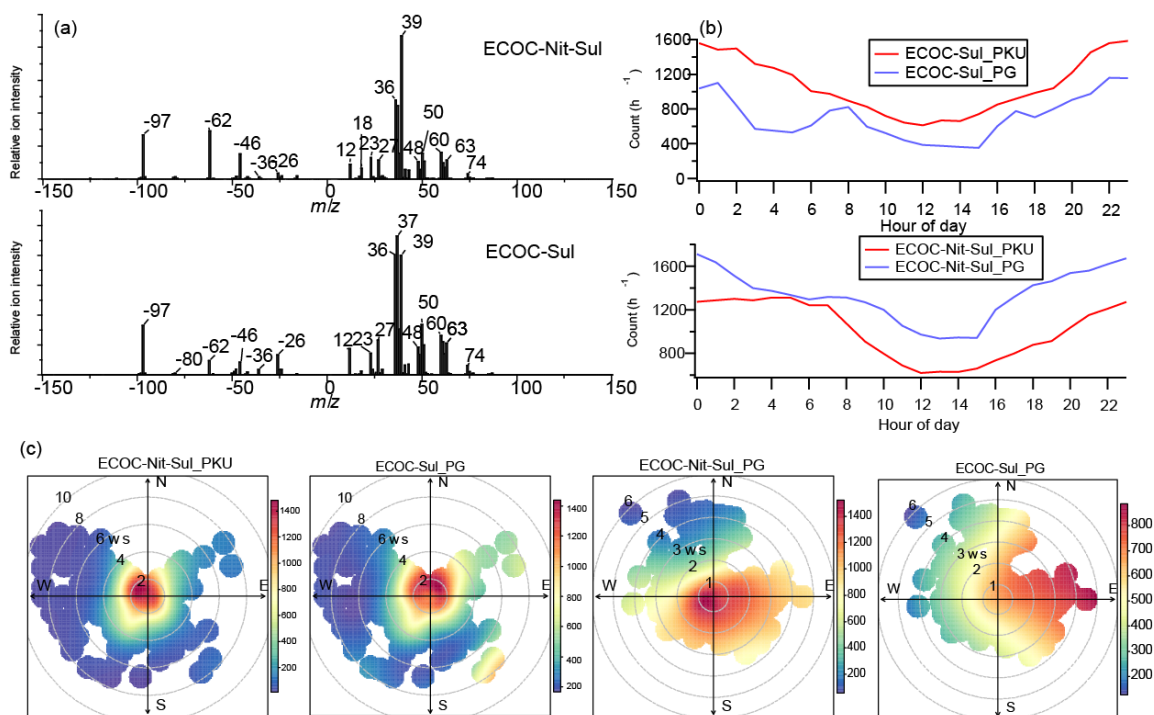


235
 236 Figure 4. (a): average mass spectra of OC-Nit and OC-Nit-Sul observed at both sites; (b):
 237 diurnal patterns of the hourly count of OC-Nit and OC-Nit-Sul at both sites; (c): polar plots
 238 of OC-Sul and OC-Nit-Sul; the grey circles indicate wind speed (m s^{-1}).

239 3.2.3 ECOC category

240 As shown in Figure 5a, the ECOC category contained two major particle types: ECOC-
 241 Nit-Sul and ECOC-Sul. The positive mass spectrum of ECOC-Nit-Sul contained C_n^+ (m/z

242 12, 24, 36...), NH_4^+ (m/z 18), C_2H_3^+ (m/z 27), K^+ (m/z 39 and 41), $\text{C}_3\text{H}_7^+/\text{C}_2\text{H}_3\text{O}^+/\text{CHNO}^+$
243 (m/z 43), C_4H_2^+ (m/z 50), and $[(\text{C}_2\text{H}_5)_2\text{NH}_2]^+$ (m/z 74); in the negative mass spectrum, ions
244 such as sulfate (m/z -80 and -97), nitrate (m/z -46 and -62), C_n^- , and CN^- (m/z -26) were
245 abundant. This mixture of EC and OC particle types was common in single particle studies.
246 ECOC could be local, and from incomplete combustion processes (Chen et al., 2017), or
247 regional transport, e.g., after aging (McGuire et al., 2011; Huang et al., 2013; Zhao et al.,
248 2019). The diurnal profile of ECOC-Sul_PG showed early morning (1:00), morning (8:00),
249 and afternoon (17:00) peaks, which is consistent with local cooking and heating patterns.
250 Also, heating activities enhanced the fraction of ECOC-Sul_PG. ECOC-Sul_PKU did not
251 show a clear diurnal profile, suggesting that ECOC-Sul_PKU was mainly a background
252 type. Similarly, ECOC-Nit-Sul_PKU and ECOC-Nit-Sul_PG were also background types
253 with less obvious diurnal variations (Dall'Osto et al., 2016). Polar plots (Figure 5c)
254 suggested that both ECOC-Nit-Sul_PKU and ECOC-Sul_PKU had both local and regional
255 sources. Wind speed up to 4 m s^{-1} could cause a transport with a distance of 346 km
256 diurnally, indicating that it was possible for the particles from Hebei province to arrive at
257 the sampling place.



258

259 Figure 5. (a): average mass spectra of ECOC-Nit and ECOC-Nit-Sul observed at both sites;
 260 (b): diurnal patterns of the hourly count of ECOC-Sul and ECOC-Nit-Sul at both sites; (c):
 261 polar plots of ECOC-Sul and ECOC-Nit-Sul; the grey circles indicate wind speed (ms^{-1}).

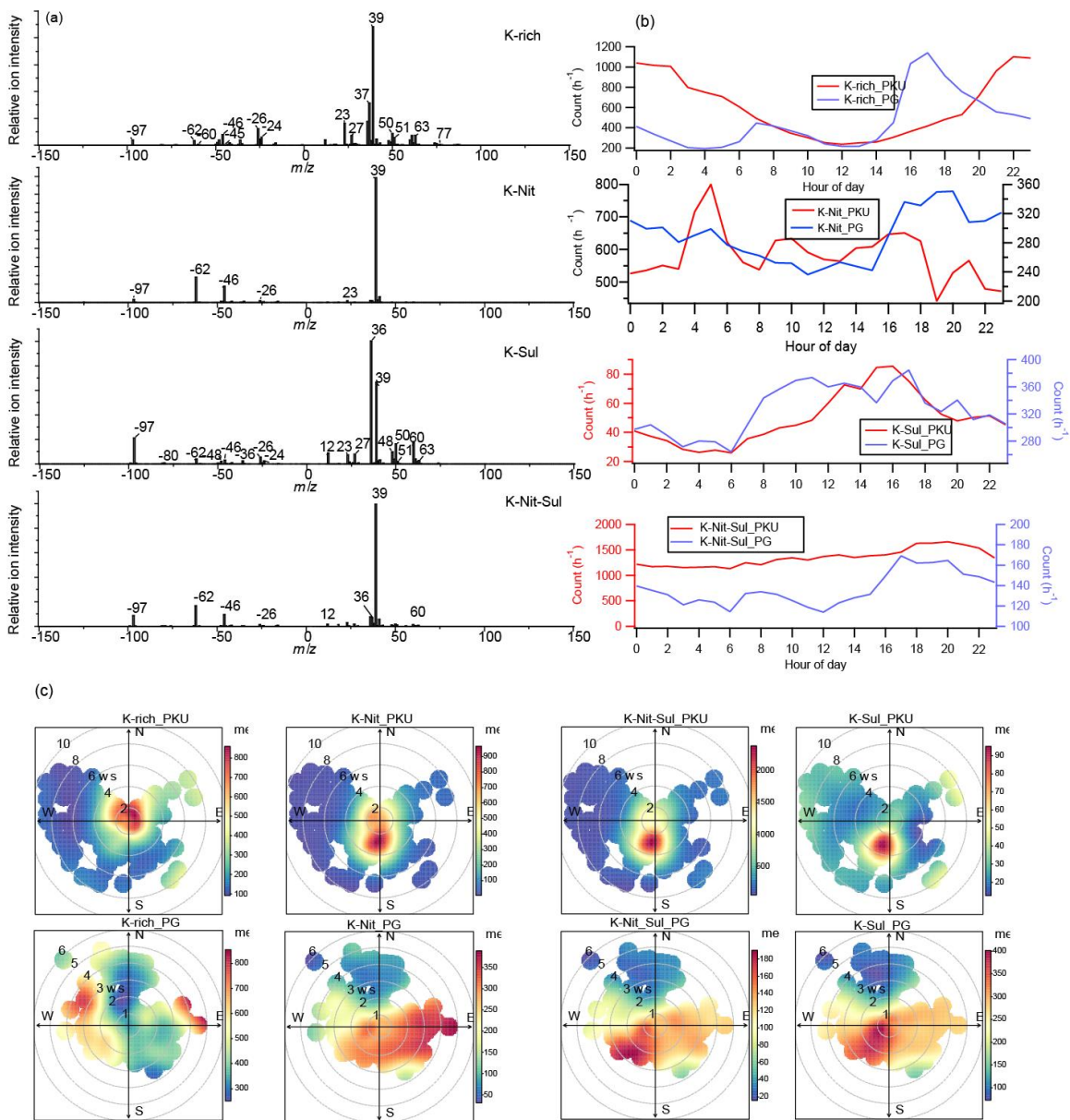
262 3.2.4 K-rich category

263 Figure 6 shows a series of potassium-rich (K) particle types. K-rich contained Na^+ (m/z 23),
 264 C_2H_3^+ (m/z 27), C_n^+ , C_3H^+ (m/z 37), K^+ , aromatic hydrocarbons (C_4H_3^+ , C_5H_3^+ , and C_6H_5^+),
 265 levoglucosan (m/z -45, -59, and -71), sulfate, and nitrate. According to the ionic intensities
 266 of sulfate and nitrate, the K-rich particle category had several branches such as K-rich, K-
 267 Nit, K-Sul, and K-Nit-Sul. K-rich particles are commonly found in biomass burning
 268 emissions (Silva et al., 1999; Pagels et al., 2013; Chen et al., 2017). Cl^- was un abundant in
 269 all K-rich particle types, suggesting that the K-rich particles had undergone aging during

270 atmospheric processing (Sullivan et al., 2007; Chen et al., 2016), but K-Nit, K-Nit-Sul, and
271 K-Sul were more processed.

272 All K-rich category particles showed different atmospheric evolution process at both PKU
273 and PG. K-rich_PKU illustrated a typical pattern that was at low levels in the daytime but
274 high levels at nighttime (22:00). As shown in Figure 6c, at an average wind speed of 3 m
275 s^{-1} , it took five hours for particles from a distance of 50 km to arrive at PKU. This is also
276 the reason why BB-related particles were abundant in urban Beijing where the household
277 BB is prohibited. The origination of K-rich_PKU was from nearby and southwest. K-
278 rich_PG, however, showed a pattern with cooking and heating activities, peaking at 7:00
279 and 17:00. The peak at 7:00 was due to the local emissions; the 17:00 could be transported
280 from a distance of 50 km at a wind speed of 3 m s^{-1} from the east and west.

281 The secondary process contributed to the early morning peak (5:00) of K-Nit_PKU due to
282 the nighttime formation of nitrate via hydrolysis of N_2O_5 in the NO_x -rich urban areas (Wang
283 et al., 2017). In the day time, after the rush hours, the number concentration of K-Nit_PKU
284 increased again via the uptake of nitrate due to day time photoactivity. K-Nit_PKU mainly
285 originated from the local and southerly areas (Figure 6c). Besides the early morning peak,
286 K-Nit_PG showed cooking and heating patterns that they were abundant when the
287 temperature was low in the early morning and afternoon. K-Nit_PG had wide originated
288 from both local and region via long-range transport.



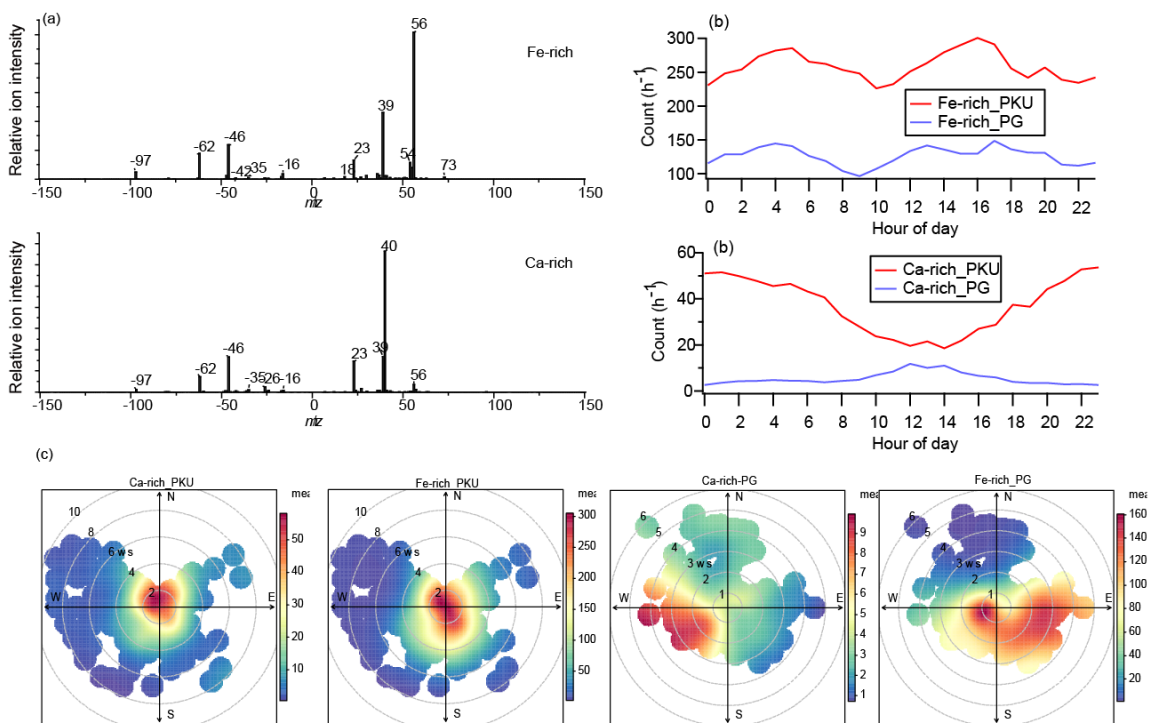
289

290 Figure 6. (a): average mass spectra of BB, K-Nit, K-Sul, and K-Nit-Sul observed at both
 291 sites; (b): diurnal patterns of the hourly count of K-rich, K-Nit, K-Sul, and K-Nit-Sul at
 292 both sites; (c): polar plots of BB, K-Nit, K-Sul, and K-Nit-Sul; the grey circles indicate
 293 wind speed (m s^{-1}).

294 3.2.5 Metal category

295 Two metal-rich particles types were identified, namely Fe-rich and Ca-rich. Fe-rich
296 contained iron (m/z 56 and 54), K^+ , Na^+ , NH_4^+ , Cl^- (m/z -35 and -37), sulfate, and nitrate.
297 Ca-rich was composed of Ca^+ (m/z 40), CaO (m/z 56), K^- , Na^+ , Cl^- , sulfate, and nitrate. As
298 shown in Figure 6b, Ca-rich_PKU (0.4%) and Ca-rich_PG (0.1%) were likely of regional
299 origin with no distinct diurnal variations. Since SiO_2^- or SiO_3^- (m/z -60 and -76) were not
300 abundant in the Ca-rich particles, they are not likely to come from dust (Silva et al., 2000).
301 According to its weak peaks during the rush hour at PKU, a possible source of the Ca-rich
302 particles was from road dust re-suspension. Such rush hour peaks were not observed at PG.

303 Fe-rich_PKU (3.1%) and Fe-rich_PG (1.8%) had similar diurnal profiles that arose in the
304 early morning when heavy-duty vehicles were allowed to enter the 5-ring expressway. The
305 peak occurred earlier at PG (4:00) than (5:00) because these vehicles got close to PG earlier
306 than to PKU. The daytime peak occurred in the afternoon at both PKU and PG when wind
307 speed was high. Therefore, there were also multiple sources for Fe-rich particles, including
308 re-suspended dust particles from traffic and fly ash from the steel industry. In Beijing,
309 daytime Fe-rich particles were reported and assigned to long-range transport and industrial
310 sources from Heibei Province (Figure 7c) (Li et al., 2014). The steel industry moved out
311 of Beijing more than a decade ago (Liu et al., 2016b). Currently, most of these steel
312 industries were located in the Heibei Province.



313

314 Figure 7. (a): average mass spectra of Fe-rich and Ca-rich observed at both sites; (b):
 315 diurnal patterns of the hourly count of Fe-rich and Ca-rich at both sites; (c): polar plots of
 316 Fe-rich and Ca-rich; the grey circles indicate wind speed (ms^{-1}).

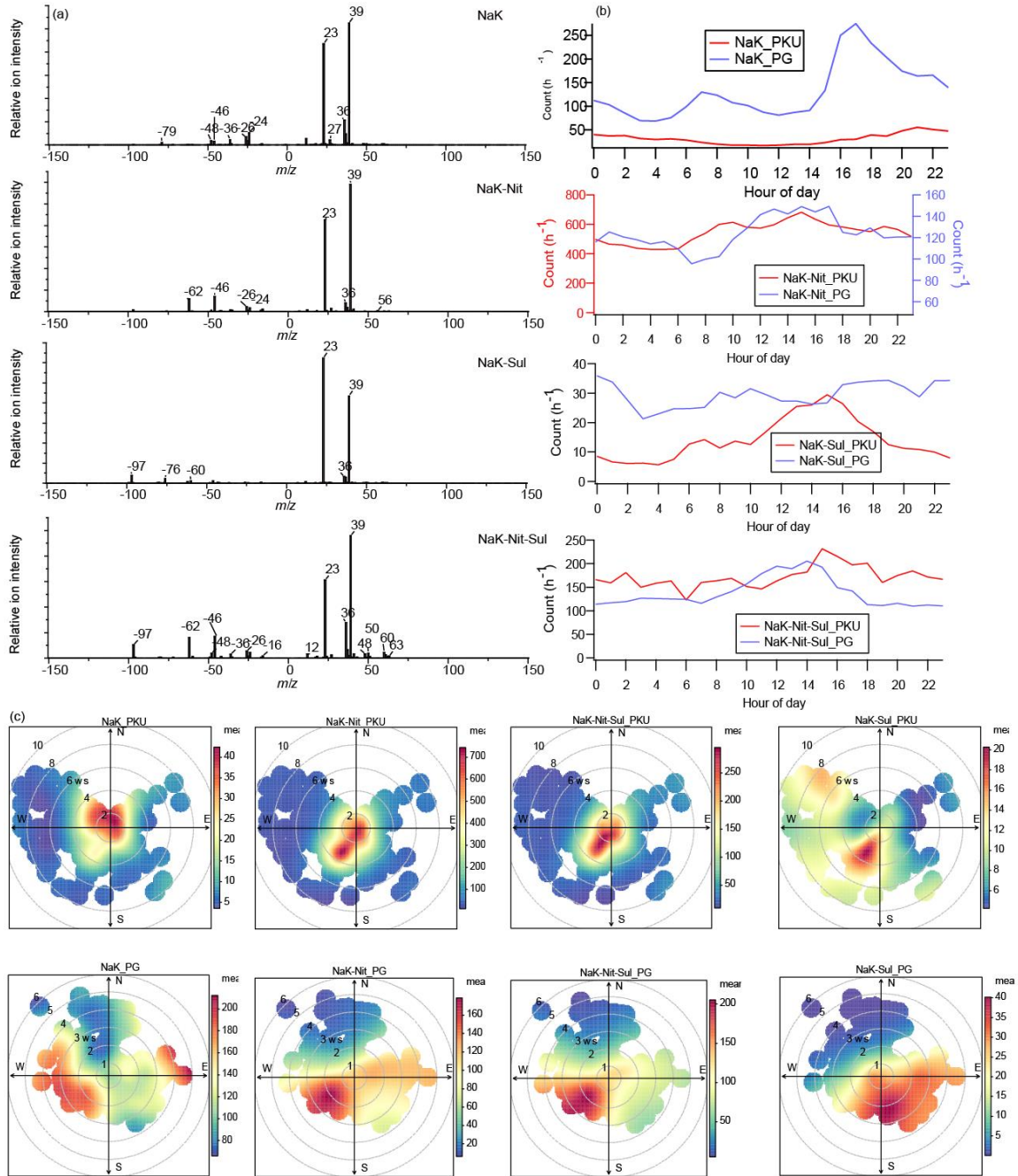
317 3.2.6 NaK category

318 As shown in Figure 8, mass spectra of NaK category contained f Na^+ , K^+ , C_n^+ , C_n^- , nitrate,
 319 and PO_3^- (m/z -79). The aged NaK particles contained strong signals of nitrate (NaK-Nit),
 320 sulfate (NaK-Sul), or both (NaK-Nit-Sul). In general, the NaK category contained stronger
 321 signals of Na^+ than the EC and K-rich categories. The NaK category may also come from
 322 incomplete solid fuel combustion processes such as coal, peat, or wood (Chen et al., 2017;
 323 Healy et al., 2010; Xu et al., 2017). NaK category was more abundant at PKU (9.5%) than
 324 PG (5.8%), suggesting a stronger contribution of emission from coal boilers (Xu et al.,

325 2017; Xu et al., 2018). Additionally, after heating began, the fraction of NaK-Nit_PG and
326 NaK-Sul-Nit_PG increased by 1.2 times (see Part II).

327 NaK_PKU showed no distinct diurnal variations, suggesting that it was a regional particle
328 type arriving at the PKU site via transport, while NaK_PG showed an apparent diurnal
329 variation consistent with cooking and heating pattern. Polar plots also suggest that they are
330 from the east and the west. NaK-Nit, with a considerable uptake of nitrate, was more
331 abundant at PKU (6.4%) than PG (1.7%). Both NaK-Nit_PKU and NaK-Nit_PG increased
332 in the afternoon when photochemical activities were most active (Figure 8c). Both of them
333 may be from regional transport (Figures 8b and 8c).

334 NaK-Sul was a minor particle type at both PG and PKU, accounting for 0.2% and 0.4%,
335 respectively. The diurnal profile of NaK-Sul_PG was also following the local cooking and
336 heating pattern, while NaK-Sul_PKU showed a typical transport pattern that became
337 abundant in the afternoon as the southwestern wind speed increased. As a heavily aged
338 particle type, NaK-Nit-Sul was transported to both PKU and PG from the southwest. In
339 short, NaK-related particle types mainly came from the solid fuel burning process, e.g.,
340 coal. Due to its different origins, it showed different levels of processing at PKU and PG,
341 respectively.



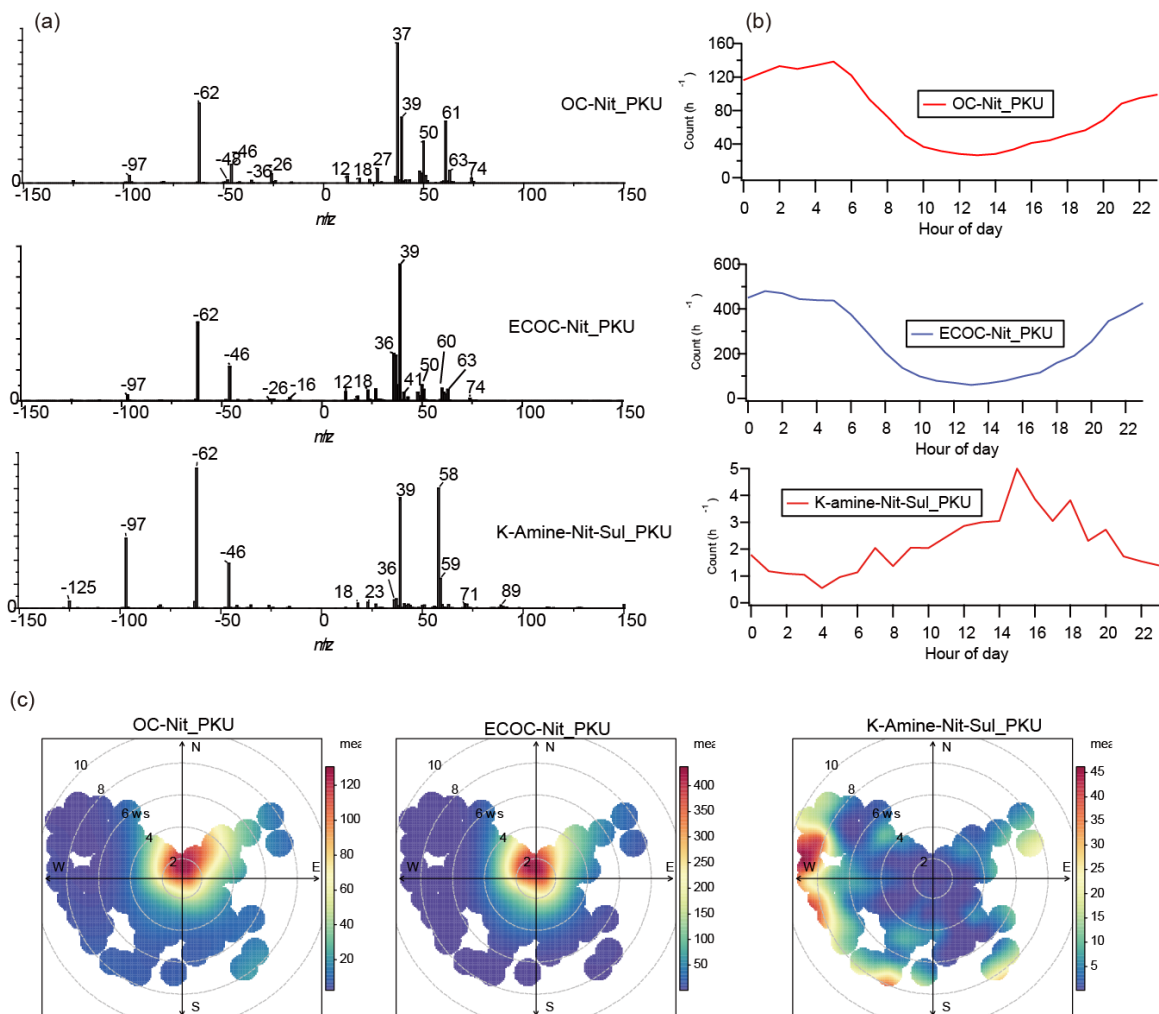
342

343 Figure 8. (a): average mass spectra of NaK, NaK-Nit, NaK-Nit-Sul, and NaK-Sul observed
 344 at both sites; (b): diurnal patterns of the hourly count of NaK, NaK-Nit, NaK-Nit-Sul, and
 345 NaK-Sul at both sites; (c): polar plots of NaK, NaK-Nit, NaK-Nit-Sul, and NaK-Sul; the
 346 grey circles indicate wind speed (m s^{-1}).

347 **3.3 Unique Particle types at the PKU site**

348 OC-Nit_PKU (0.9%) and ECOC-Nit_PKU (3.1%) with strong ion intensities of nitrate
349 were observed at the PKU site. OC-Nit_PKU and ECOC-Nit_PKU showed a peak at night
350 than at daytime, similar to the diurnal profiles of OC-Nit-Sul_PKU and ECOC-Nit-
351 Sul_PKU. Such nitrate-rich particle types could have come from the uptake of nitrate in
352 OC and ECOC(Qin et al., 2012; Chen et al., 2016). Polar plots suggest that both types were
353 formed locally when the wind speed was lower than 4 ms^{-1} . The NO_x -rich environment in
354 urban Beijing provides a favorable condition for nitrate formation at night (Wang et al.,
355 2016a; Zou et al., 2015; Shi et al., 2019).

356 A minor amount (0.10%) of amine-containing particles was observed at the PKU site, and
357 trimethylamine ion fragments (m/z 58 and 59) were influential in the mass spectrum of K-
358 amine-Nit-Sul_PKU (Figure 9a). The diurnal profile of K-amine-Nit-Sul_PKU showed an
359 afternoon peak, indicating a regional source (Figure 9c). K-amine-Nit-Sul_PKU was
360 transported to the site from nearby locations. The amines may come from animal husbandry,
361 BB, traffic, or vegetation (Chen et al., 2019). Amines were ubiquitous in the atmospheric
362 environment, playing essential roles in new particle formation and growth, as well as fog
363 and cloud processing (Ge et al., 2011; Chen et al., 2019).



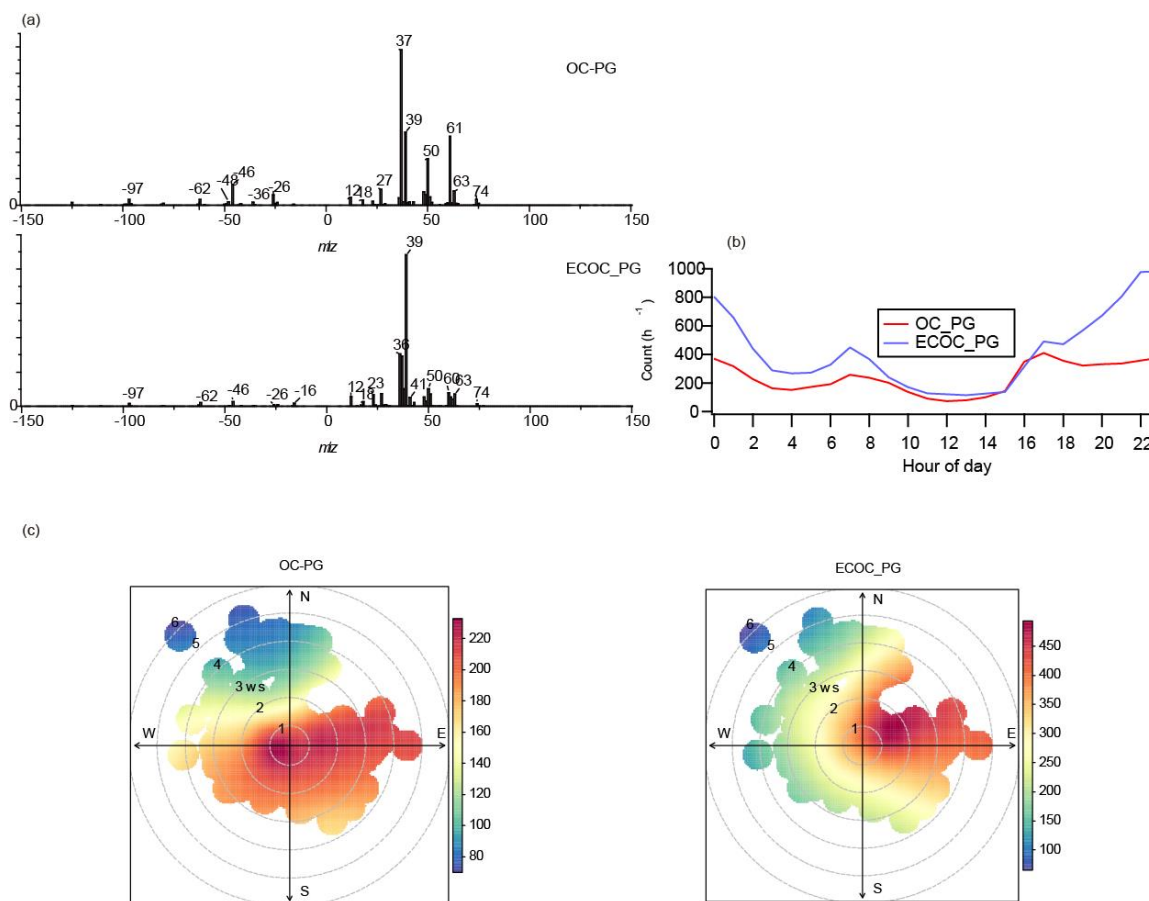
364

365 Figure 9. (a): average mass spectra of OC-Nit_PKU, ECOC-Nit_PKU, and K-amine-Nit-
 366 Sul_PKU observed at the PKU site; (b): diurnal patterns of the hourly count of OC-
 367 Nit_PKU, ECOC-Nit_PKU, and K-amine-Nit-Sul_PKU at the PKU site; (c): polar plots of
 368 OC-Nit_PKU, ECOC-Nit_PKU, and K-amine-Nit-Sul_PKU, and the grey circles indicate
 369 wind speed (m s⁻¹).

370 3.4 Unique Particle types at the PG site

371 OC_PG (5.9%) and ECOC_PG (3.3%) were only observed at the rural site PG (Figure 10).
 372 The major components of these two types were consistent with the OC and ECOC

373 categories, respectively, but with limited uptake of sulfate and nitrate, suggesting that they
 374 were possibly freshly emitted particles(Peng et al., 2020b). Their diurnal profiles are
 375 consistent with cooking and heating patterns which peaked at 07:00 in the morning and
 376 17:00. Polar plots suggest that OC_PG mainly came from nearby and other remote areas
 377 in all directions except the north. ECOC mainly came from the east of the PG site. These
 378 results supported the assumption that the two types were mainly from local emission
 379 sources. Also, the emission of OC_PG and ECOC_PG is popular in the region.



380

381 Figure 10. (a) Average mass spectra of OC_PG and ECOC_PG, (c) diurnal plots of OC_PG
 382 and ECOC_PG, and (c) polar plots of OC_PG and ECOC_PG. All these particle types
 383 appeared at the PG site.

384 **4. Discussion**

385 Multiple source apportionment models have been used in Beijing to quantify the sources
386 of particles (Sun et al., 2014a; Xu et al., 2015; Zhai et al., 2016). Biomass burning, coal
387 combustion, traffic, and dust are the key sources of PM (Sun et al., 2014a; Liu et al., 2018;
388 Huang et al., 2014). Multiple studies confirmed that biomass burning is an essential source
389 of PM in urban Beijing (Gao et al., 2014; Huang et al., 2014; Sun et al., 2014a; Zheng et
390 al., 2017). In this study, biomass burning, and other solid fuel burning were identified as
391 crucial sources of PM in not only urban but also rural areas of Beijing. We observed that
392 BB-related particles (K-rich category) were more abundant at PG than at PKU. In particular,
393 we found fresh-emitted K-containing particles at the Pinggu site, confirmed the importance
394 of local emissions to PM. Furthermore, K-containing particles in the urban area were more
395 aged, suggested that they are aged and mostly from the surrounding areas. The result is
396 consistent with the results from (Liu et al., 2019b) based on a combined receptor and
397 footprint models. Nevertheless, household emissions in the BHT region caused 32% and
398 15% of primary PM_{2.5} and SO₂. These studies have proved the importance of household
399 emission from BB in the BHT area (Liu et al., 2016a). Especially at the PG site, the ambient
400 PM was mainly controlled by long-range transport and household emissions from cooking
401 and heating.

402 Due to the nature of SPAMS, the chemical composition of PM cannot be precisely
403 quantified. However, single particle aerosol mass spectrometers have advantages in
404 studying the chemical composition, mixing state, source, and process of particles (Pratt and
405 Prather, 2012). Mass-based technologies can not differentiate the origin of the bulk of
406 nitrate, whether it is transported or formed locally. Indeed, single particle types in urban

407 Beijing have been reported in previous studies (Li et al., 2014; Liu et al., 2016b), and the
408 major types are consistent with this study. However, in this study, we adopted a cluster
409 strategy considering the relative ion peak area of sulfate and nitrate as indicators of particle
410 processing. Therefore, more detail could be extracted from both two simultaneous datasets.
411 We confirmed that the source, origination, and processes were different for these particles
412 in the urban and rural areas. For example, the seriously processed particles, such as K-Nit-
413 Sul, OC-Nit-Sul, and NaK-Nit-Sul, acted with no distinct diurnal patterns as background
414 or regional sources (Xie et al., 2019). The processed particles, such as OC-Nit, ECOC-Nit,
415 and NaK-Nit, were affected by emissions and secondary formations.

416 The emission and transport patterns were different in the urban and rural areas, resulting in
417 different characteristics of PM. For example, EC particles were a key component at PKU
418 (18.2% in total), but a minor particle type at PG (5.6%). Meanwhile, in the urban area of
419 Beijing, direct emission of K-rich particles should be small due to strict control measures;
420 thus, the K-Nit-Sul particles are mainly from long-range transport. Transported particles
421 were aged and commonly coated a thick layer of nitrate and sulfate, but the local particles
422 were affected by both emission and the near-surface aging process. For example, at PKU,
423 the primary emission sources were traffic and central heating supply, causing a NO_x-rich
424 region in which freshly-emitted particle types could undergo processing due to the uptake
425 of nitrate (Wang et al., 2016a). In the nearby villages of PG, domestic heating and cooking
426 were the major contributors of primary particles when the temperature was low in the
427 morning and afternoon, resulting in the emission of multiple primary particle types such as
428 OC_PG and ECOC_PG. In short, the characteristics of PM in urban and rural areas of

429 Beijing were affected by local emissions and interacted with each other due to regional
430 transport.

431 SO₂ was controlled strictly in Beijing. However, the emission of SO₂ is still significant in the nearby
432 Hebei and Shandong provinces (Shi et al. 2019). The different control measures produced a low
433 concentration area of SO₂ around Beijing. The sulfate-rich particle types, such as EC-Sul, OC-Sul,
434 K-Sul, and NaK-Sul, arrived at the PKU site when wind speed was commonly high (> 3m s⁻¹). The
435 wind directions, along with the transport of sulfate-rich particles were the east, southwest, and south.
436 In these directions, Sulfate was either primarily emitted from coal burning from residential heating,
437 power generation as well as industry, or secondarily uptake on the pre-existing particles (Zhang et
438 al., 2015). Likewise, a part of the sulfate-rich particle arrived at the PG site when wind speed was
439 high. However, the locally formed were also pronounced, especially for ECOC-Sul, K-Sul, and
440 NaK-Sul. As discussed in Section 3, ECOC-Sul and NaK-Sul were mainly from the coal burning
441 for residential heating. The K-Sul was formed due to the uptake of secondary sulfate. Conclusively,
442 the particulate characterization in rural areas around Beijing is influenced significantly by
443 residential coal burning.

444 Secondary nitrate formation is still a critical issue in Beijing. The daytime arising of nitrate
445 has been reported in studies (Sun et al., 2013), and we also found a similar predominant of
446 nitrogen-containing particles in this study. Recent studies have reported the early morning
447 peaks of nitrate using a soot particle aerosol mass spectrometer (SP-AMS) (Wang et al.,
448 2019), which is consistent with our results. Interestingly, the early morning peak was only
449 observed for several particle types at both sites, including EC-Nit_PKU, K-Nit_PKU, EC-
450 Nit-Sul-PG, and EC-Nit_PG. This result is not surprising because PG is also a NO₂-rich
451 region (Shi et al., 2019). The increasing contribution of nitrate-containing particles
452 suggests the role of night chemistry in nitrate uptake on particles. Wang et al. (2017)

453 revealed the importance of night N_2O_5 chemistry on nocturnal nitrate formation in the
454 urban area of Beijing. The heterogeneous hydrolysis of N_2O_5 was most favorable when NO
455 was at a low level. Moreover, the polar plots suggested a small role of long-range transport
456 to the nitrate in individual particles. The contribution of local traffic was insignificant at
457 the PG site as it was far from highways and major roads, the nighttime formation of nitrate
458 appeared to be important in PG as well.

459 **5. Conclusion**

460 Two SPAMs were simultaneously deployed at urban and rural sites in Beijing in order to
461 characterize PM during wintertime. The results at both sites indicate that they shared 17
462 types of common clusters, most of which belonged to particle categories such as EC, OC,
463 ECOC, BB, and NaK. The origins and sources of these particle types at both sampling sites
464 are also comprehensively analyzed. Most of the processed PM, including EC-Nit-Sul_PKU,
465 ECOC-Nit-Sul_PKU, and NaK-Nit-Sul_PKU, were aged locally in a NO_x -rich
466 environment, while EC-Nit-Sul_PG, ECOC-Nit-Sul_PG, NaK-Nit-Sul_PG, and OC-Nit-
467 Sul_PG were regional. Domestic heating in the rural area was found to be an important
468 source of PM, and such heating activities typically caused three diurnal peaks in the early
469 morning, morning, and afternoon (after sunset). Moreover, the early morning peak of
470 nitrate was observed at both sites, suggesting the contribution of the heterogeneous
471 hydrolysis of N_2O_5 in the dark during the winter. The insights gained in this study can
472 provide useful references for understanding the relationship between regional transport and
473 local aging in both urban and rural areas in Beijing. In Part II, we focus on haze events

474 observed at both sites and attempt to determine the effects of heating activities and possible
475 regional transport between PKU and PG.

476 *Data availability.* All data described in this study are available upon request from the
477 corresponding authors.

478 *Author contributions.* FY, MZ, TZ, QZ, and KH designed the experiments; YC, JC, ZW,
479 MT, CP, and HY carried them out; XYang, XYao, YL, GS, and ZS analyzed the
480 experimental data; YC prepared the manuscript with contributions from all coauthors.

481 *Competing interests.* The authors declare that they have no conflict of interest.

482 *Acknowledgments.* We are grateful for financial support from the National Natural Science
483 Foundation of China (Grant No. 4170030287 and 81571130100). ZS acknowledges
484 funding from NERC (NE/N007190/1 and NE/R005281/1).

485 **References**

486 Bi, X., Zhang, G., Li, L., Wang, X., Li, M., Sheng, G., Fu, J., and Zhou, Z.: Mixing state
487 of biomass burning particles by single particle aerosol mass spectrometer in the urban area
488 of PRD, China, *Atmos. Environ.*, 45, 3447-3453, 10.1016/j.atmosenv.2011.03.034, 2011.

489 Cai, J., Wang, J., Zhang, Y., Tian, H., Zhu, C., Gross, D. S., Hu, M., Hao, J., He, K., and
490 Wang, S.: Source apportionment of Pb-containing particles in Beijing during January 2013,
491 *Environ Pollut*, 226, 30-40, 2017.

492 Chen, Y., Cao, J., Huang, R., Yang, F., Wang, Q., and Wang, Y.: Characterization, mixing
493 state, and evolution of urban single particles in Xi'an (China) during wintertime haze days,
494 *Sci. Total Environ.*, 573, 937-945, 10.1016/j.scitotenv.2016.08.151, 2016.

495 Chen, Y., Wenger, J. C., Yang, F., Cao, J., Huang, R., Shi, G., Zhang, S., Tian, M., and
496 Wang, H.: Source characterization of urban particles from meat smoking activities in
497 Chongqing, China using single particle aerosol mass spectrometry, *Environ. Pollut.*, 228,
498 92-101, 10.1016/j.envpol.2017.05.022, 2017.

499 Chen, Y., Tian, M., Huang, R.-J., Shi, G., Wang, H., Peng, C., Cao, J., Wang, Q., Zhang,
500 S., Guo, D., Zhang, L., and Yang, F.: Characterization of urban amine-containing particles
501 in southwestern China: seasonal variation, source, and processing, *Atmos. Chem. Phys.*,
502 19, 3245-3255, 10.5194/acp-19-3245-2019, 2019.

503 Cheng, Y., Zheng, G., Wei, C., Mu, Q., Zheng, B., Wang, Z., Gao, M., Zhang, Q., He, K.,
504 and Carmichael, G.: Reactive nitrogen chemistry in aerosol water as a source of sulfate
505 during haze events in China, *Science Advances*, 2, e1601530, 2016.

506 Dall'Osto, M., Beddows, D., McGillicuddy, E. J., Esser-Gietl, J. K., Harrison, R. M., and
507 Wenger, J. C.: On the simultaneous deployment of two single-particle mass spectrometers
508 at an urban background and a roadside site during SAPUSS, *Atmos. Chem. Phys.*, 16,
509 9693-9710, 2016.

510 Dallosto, M., and Harrison, R.: Chemical characterisation of single airborne particles in
511 Athens (Greece) by ATOFMS, *Atmos. Environ.*, 40, 7614-7631,
512 10.1016/j.atmosenv.2006.06.053, 2006.

513 Day, D. A., Liu, S., Russell, L. M., and Ziemann, P. J.: Organonitrate group concentrations
514 in submicron particles with high nitrate and organic fractions in coastal southern California,
515 *Atmos Environ*, 44, 1970-1979, 10.1016/j.atmosenv.2010.02.045, 2010.

516 Du, W., Zhao, J., Wang, Y., Zhang, Y., Wang, Q., Xu, W., Chen, C., Han, T., Zhang, F.,
517 Li, Z., Fu, P., Li, J., Wang, Z., and Sun, Y.: Simultaneous measurements of particle number
518 size distributions at ground level and 260 m on a meteorological tower in urban Beijing,
519 China, *Atmos. Chem. Phys.*, 17, 6797-6811, 10.5194/acp-17-6797-2017, 2017.

520 Gao, J., Zhang, Y., Zhang, M., Zhang, J., Wang, S., Tao, J., Wang, H., Luo, D., Chai, F.,
521 and Ren, C.: Photochemical properties and source of pollutants during continuous pollution
522 episodes in Beijing, October, 2011, *J Environ Sci-China*, 26, 44-53, 10.1016/s1001-
523 0742(13)60379-4, 2014.

524 Gard, E., Mayer, J. E., Morrical, B. D., Dienes, T., Fergenson, D. P., and Prather, K. A.:
525 Real-time analysis of individual atmospheric aerosol particles: Design and performance of
526 a portable ATOFMS, *Anal. Chem.*, 69, 4083-4091, 1997.

527 Ge, X., Wexler, A. S., and Clegg, S. L.: Atmospheric amines – Part I. A review, *Atmos.*
528 *Environ.*, 45, 524-546, 10.1016/j.atmosenv.2010.10.012, 2011.

529 Guo, S., Hu, M., Guo, Q., Zhang, X., Zheng, M., Zheng, J., Chang, C. C., Schauer, J. J.,
530 and Zhang, R.: Primary sources and secondary formation of organic aerosols in Beijing,
531 China, *Environ. Sci. Technol.*, 46, 9846-9853, 10.1021/es2042564, 2012.

532 Guo, S., Hu, M., Zamora, M. L., Peng, J., Shang, D., Zheng, J., Du, Z., Wu, Z., Shao, M.,
533 Zeng, L., Molina, M. J., and Zhang, R.: Elucidating severe urban haze formation in China,
534 *Proc Natl Acad Sci U S A*, 111, 17373-17378, 10.1073/pnas.1419604111, 2014.

535 He, K., Yang, F., Ma, Y., Zhang, Q., Yao, X., Chan, C. K., Cadle, S., Chan, T., and Mulawa,
536 P.: The characteristics of PM_{2.5} in Beijing, China, *Atmos. Environ.*, 35, 4959-4970,
537 10.1016/s1352-2310(01)00301-6, 2001.

538 Healy, R. M., Hellebust, S., Kourtchev, I., Allan, A., and Connor, I. P., Bell, J.
539 M., Healy, D. A., Sodeau, J. R., and Wenger, J. C.: Source apportionment of PM_{2.5} in
540 Cork Harbour, Ireland using a combination of single particle mass spectrometry and
541 quantitative semi-continuous measurements, *Atmos. Chem. Phys.*, 10, 9593-9613,
542 10.5194/acp-10-9593-2010, 2010.

543 Healy, R. M., Sciare, J., Poulain, L., Kamili, K., Merkel, M., Müller, T., Wiedensohler, A.,
544 Eckhardt, S., Stohl, A., Sarda-Estève, R., McGillicuddy, E., and Connor, I. P.,
545 Sodeau, J. R., and Wenger, J. C.: Sources and mixing state of size-resolved elemental
546 carbon particles in a European megacity: Paris, *Atmos. Chem. Phys.*, 12, 1681-1700,
547 10.5194/acp-12-1681-2012, 2012.

548 Huang, M., Hao, L., Guo, X., Hu, C., Gu, X., Zhao, W., Wang, Z., Fang, L., and Zhang,
549 W.: Characterization of secondary organic aerosol particles using aerosol laser time-of-
550 flight mass spectrometer coupled with FCM clustering algorithm, *Atmos. Environ.*, 64, 85-
551 94, 10.1016/j.atmosenv.2012.09.044, 2013.

552 Huang, R. J., Zhang, Y., Bozzetti, C., Ho, K. F., Cao, J. J., Han, Y., Daellenbach, K. R.,
553 Slowik, J. G., Platt, S. M., Canonaco, F., Zotter, P., Wolf, R., Pieber, S. M., Bruns, E. A.,
554 Crippa, M., Ciarelli, G., Piazzalunga, A., Schwikowski, M., Abbaszade, G., Schnelle-Kreis,
555 J., Zimmermann, R., An, Z., Szidat, S., Baltensperger, U., El Haddad, I., and Prevot, A. S.:
556 High secondary aerosol contribution to particulate pollution during haze events in China,
557 *Nature*, 514, 218-222, 10.1038/nature13774, 2014.

558 Huang, X.-F., He, L.-Y., Hu, M., and Zhang, Y.-H.: Annual variation of particulate organic
559 compounds in PM_{2.5} in the urban atmosphere of Beijing, *Atmos. Environ.*, 40, 2449-2458,
560 10.1016/j.atmosenv.2005.12.039, 2006.

561 Huang, X. F., He, L. Y., Hu, M., Canagaratna, M. R., Sun, Y., Zhang, Q., Zhu, T., Xue, L.,
562 Zeng, L. W., Liu, X. G., Zhang, Y. H., Jayne, J. T., Ng, N. L., and Worsnop, D. R.: Highly
563 time-resolved chemical characterization of atmospheric submicron particles during 2008
564 Beijing Olympic Games using an Aerodyne High-Resolution Aerosol Mass Spectrometer,
565 *Atmos. Chem. Phys.*, 10, 8933-8945, 10.5194/acp-10-8933-2010, 2010.

566 Li, L., Huang, Z., Dong, J., Li, M., Gao, W., Nian, H., Fu, Z., Zhang, G., Bi, X., Cheng, P.,
567 and Zhou, Z.: Real time bipolar time-of-flight mass spectrometer for analyzing single
568 aerosol particles, *Int. J. Mass spectrom.*, 303, 118-124, 10.1016/j.ijms.2011.01.017, 2011.

569 Li, L., Li, M., Huang, Z., Gao, W., Nian, H., Fu, Z., Gao, J., Chai, F., and Zhou, Z.:
570 Ambient particle characterization by single particle aerosol mass spectrometry in an urban
571 area of Beijing, *Atmos. Environ.*, 94, 323-331, 10.1016/j.atmosenv.2014.03.048, 2014.

572 Li, P., Yan, R., Yu, S., Wang, S., Liu, W., and Bao, H.: Reinstate regional transport of
573 PM_{2.5} as a major cause of severe haze in Beijing, *Proc Natl Acad Sci U S A*, 112, E2739-
574 2740, 10.1073/pnas.1502596112, 2015a.

575 Li, P., Yan, R., Yu, S., Wang, S., Liu, W., and Bao, H.: Reinstate regional transport of
576 PM_{2.5} as a major cause of severe haze in Beijing, *Proc Natl Acad Sci U S A*, 112, 2015b.

577 Liu, D., Joshi, R., Wang, J., Yu, C., Allan, J. D., Coe, H., Flynn, M. J., Xie, C., Lee, J.,
578 Squires, F., Kotthaus, S., Grimmond, S., Ge, X., Sun, Y., and Fu, P.: Contrasting physical

579 properties of black carbon in urban Beijing between winter and summer, *Atmos. Chem.*
580 *Phys.*, 19, 6749-6769, 10.5194/acp-19-6749-2019, 2019a.

581 Liu, J., Mauzerall, D. L., Chen, Q., Zhang, Q., Song, Y., Peng, W., Klimont, Z., Qiu, X.,
582 Zhang, S., Hu, M., Lin, W., Smith, K. R., and Zhu, T.: Air pollutant emissions from
583 Chinese households: A major and underappreciated ambient pollution source, *Proceedings*
584 *of the National Academy of Sciences*, 113, 7756-7761, 10.1073/pnas.1604537113, 2016a.

585 Liu, L., Wang, Y., Du, S., Zhang, W., Hou, L., Vedal, S., Han, B., Yang, W., Chen, M.,
586 and Bai, Z.: Characteristics of atmospheric single particles during haze periods in a typical
587 urban area of Beijing: A case study in October, 2014, *J Environ Sci-China*, 40, 145-153,
588 10.1016/j.jes.2015.10.027, 2016b.

589 Liu, Y., Zheng, M., Yu, M., Cai, X., Du, H., Li, J., Zhou, T., Yan, C., Wang, X., Shi, Z.,
590 Harrison, R. M., Zhang, Q., and He, K.: High Time Resolution Source Apportionment of
591 $PM_{2.5}$ in Beijing with Multiple Models, *Atmospheric Chemistry*
592 *and Physics Discussions*, 2018, 1-31, 10.5194/acp-2018-1234, 2018.

593 Liu, Y., Zheng, M., Yu, M., Cai, X., Du, H., Li, J., Zhou, T., Yan, C., Wang, X., Shi, Z.,
594 Harrison, R. M., Zhang, Q., and He, K.: High-time-resolution source apportionment of
595 $PM_{2.5}$ in Beijing with multiple models, *Atmos Chem Phys*, 19,
596 6595-6609, 10.5194/acp-19-6595-2019, 2019b.

597 Ma, L., Li, M., Huang, Z., Li, L., Gao, W., Nian, H., Zou, L., Fu, Z., Gao, J., Chai, F., and
598 Zhou, Z.: Real time analysis of lead-containing atmospheric particles in Beijing during
599 springtime by single particle aerosol mass spectrometry, *Chemosphere*, 154, 454-462,
600 10.1016/j.chemosphere.2016.04.001, 2016.

601 McGuire, M. L., Jeong, C. H., Slowik, J. G., Chang, R. Y. W., Corbin, J. C., Lu, G., Mihele,
602 C., Rehbein, P. J. G., Sills, D. M. L., Abbatt, J. P. D., Brook, J. R., and Evans, G. J.:
603 Elucidating determinants of aerosol composition through particle-type-based receptor
604 modeling, *Atmos. Chem. Phys.*, 11, 8133-8155, 10.5194/acp-11-8133-2011, 2011.

605 Pagels, J., Dutcher, D. D., Stolzenburg, M. R., McMurry, P. H., Gälli, M. E., and Gross, D.
606 S.: Fine-particle emissions from solid biofuel combustion studied with single-particle mass
607 spectrometry: Identification of markers for organics, soot, and ash components, *J. Geophys.*
608 *Res. Atmos.*, 118, 859-870, 10.1029/2012jd018389, 2013.

609 Peng, C., Tian, M., Wang, X., Yang, F., Shi, G., Huang, R.-J., Yao, X., Wang, Q., Zhai,
610 C., Zhang, S., Qian, R., Cao, J., and Chen, Y.: Light absorption of brown carbon in PM_{2.5}
611 in the Three Gorges Reservoir region, southwestern China: Implications of biomass
612 burning and secondary formation, *Atmos. Environ.*, 229, 117409,
613 <https://doi.org/10.1016/j.atmosenv.2020.117409>, 2020a.

614 Peng, C., Yang, F., Tian, M., Shi, G., Li, L., Huang, R. J., Yao, X., Luo, B., Zhai, C., and
615 Chen, Y.: Brown carbon aerosol in two megacities in the Sichuan Basin of southwestern
616 China: Light absorption properties and implications, *Sci. Total Environ.*, 719, 137483,
617 10.1016/j.scitotenv.2020.137483, 2020b.

618 Pratt, K. A., and Prather, K. A.: Mass spectrometry of atmospheric aerosols--recent
619 developments and applications. Part II: On-line mass spectrometry techniques, *Mass*
620 *Spectrom. Rev.*, 31, 17-48, 10.1002/mas.20330, 2012.

621 Qin, X., Pratt, K. A., Shields, L. G., Toner, S. M., and Prather, K. A.: Seasonal comparisons
622 of single-particle chemical mixing state in Riverside, CA, *Atmos. Environ.*, *59*, 587-596,
623 10.1016/j.atmosenv.2012.05.032, 2012.

624 Shi, Z., Vu, T., Kotthaus, S., Harrison, R. M., Grimmond, S., Yue, S., Zhu, T., Lee, J., Han,
625 Y., Demuzere, M., Dunmore, R. E., Ren, L., Liu, D., Wang, Y., Wild, O., Allan, J., Acton,
626 W. J., Barlow, J., Barratt, B., Beddows, D., Bloss, W. J., Calzolari, G., Carruthers, D.,
627 Carslaw, D. C., Chan, Q., Chatzidiakou, L., Chen, Y., Crilley, L., Coe, H., Dai, T., Doherty,
628 R., Duan, F., Fu, P., Ge, B., Ge, M., Guan, D., Hamilton, J. F., He, K., Heal, M., Heard,
629 D., Hewitt, C. N., Hollaway, M., Hu, M., Ji, D., Jiang, X., Jones, R., Kalberer, M., Kelly,
630 F. J., Kramer, L., Langford, B., Lin, C., Lewis, A. C., Li, J., Li, W., Liu, H., Liu, J., Loh,
631 M., Lu, K., Lucarelli, F., Mann, G., McFiggans, G., Miller, M. R., Mills, G., Monk, P.,
632 Nemitz, E., O'Connor, F., Ouyang, B., Palmer, P. I., Percival, C., Popoola, O., Reeves, C.,
633 Rickard, A. R., Shao, L., Shi, G., Spracklen, D., Stevenson, D., Sun, Y., Sun, Z., Tao, S.,
634 Tong, S., Wang, Q., Wang, W., Wang, X., Wang, X., Wang, Z., Wei, L., Whalley, L., Wu,
635 X., Wu, Z., Xie, P., Yang, F., Zhang, Q., Zhang, Y., Zhang, Y., and Zheng, M.: Introduction
636 to the special issue “In-depth study of air pollution sources and processes within Beijing
637 and its surrounding region (APHH-Beijing)”, *Atmos. Chem. Phys.*, *19*, 7519-7546,
638 10.5194/acp-19-7519-2019, 2019.

639 Silva, P. J., Liu, D.-Y., Noble, C. A., and Prather, K. A.: Size and Chemical
640 Characterization of Individual Particles Resulting from Biomass Burning of Local
641 Southern California Species, *Environ. Sci. Technol.*, *33*, 3068-3076, 10.1021/es980544p,
642 1999.

643 Silva, P. J., Carlin, R. A., and Prather, K. A.: Single particle analysis of suspended soil dust
644 from Southern California, *Atmos Environ*, 34, 1811-1820, 10.1016/S1352-
645 2310(99)00338-6, 2000.

646 Sodeman, D. A., Toner, S. M., and Prather, K. A.: Determination of single particle mass
647 spectral signatures from light-duty vehicle emissions, *Environ. Sci. Technol.*, 39, 4569-
648 4580, 10.1021/es0489947, 2005.

649 Sullivan, R. C., Guazzotti, S. A., Sodeman, D. A., Tang, Y., Carmichael, G. R., and Prather,
650 K. A.: Mineral dust is a sink for chlorine in the marine boundary layer, *Atmos. Environ.*,
651 41, 7166-7179, 10.1016/j.atmosenv.2007.05.047, 2007.

652 Sun, Y., Jiang, Q., Wang, Z., Fu, P., Li, J., Yang, T., and Yin, Y.: Investigation of the
653 sources and evolution processes of severe haze pollution in Beijing in January 2013, *J*
654 *Geophys Res*, 119, 4380-4398, 2014a.

655 Sun, Y., Jiang, Q., Wang, Z., Fu, P., Li, J., Yang, T., and Yin, Y.: Investigation of the
656 sources and evolution processes of severe haze pollution in Beijing in January 2013, *J.*
657 *Geophys. Res. Atmos.*, 119, 4380-4398, 10.1002/2014jd021641, 2014b.

658 Sun, Y. L., Wang, Z. F., Fu, P. Q., Yang, T., Jiang, Q., Dong, H. B., Li, J., and Jia, J. J.:
659 Aerosol composition, sources and processes during wintertime in Beijing, China, *Atmos.*
660 *Chem. Phys.*, 13, 4577-4592, 10.5194/acp-13-4577-2013, 2013.

661 Tao, S., Wang, X., Chen, H., Yang, X., Li, M., Li, L., and Zhou, Z.: Single particle analysis
662 of ambient aerosols in Shanghai during the World Exposition, 2010: two case studies, *Front*
663 *Environ Sci En*, 5, 391-401, 10.1007/s11783-011-0355-x, 2011.

664 Toner, S. M., Sodeman, D. a., and Prather, K. a.: Single particle characterization of
665 ultrafine and accumulation mode particles from heavy duty diesel vehicles using aerosol
666 time-of-flight mass spectrometry, *Environ. Sci. Technol.*, 40, 3912-3921, 2006.

667 Toner, S. M., Shields, L. G., Sodeman, D. A., and Prather, K. A.: Using mass spectral
668 source signatures to apportion exhaust particles from gasoline and diesel powered vehicles
669 in a freeway study using UF-ATOFMS, *Atmos. Environ.*, 42, 568-581,
670 10.1016/j.atmosenv.2007.08.005, 2008.

671 Wang, G., Zhang, R., Gomez, M. E., Yang, L., Levy Zamora, M., Hu, M., Lin, Y., Peng,
672 J., Guo, S., Meng, J., Li, J., Cheng, C., Hu, T., Ren, Y., Wang, Y., Gao, J., Cao, J., An, Z.,
673 Zhou, W., Li, G., Wang, J., Tian, P., Marrero-Ortiz, W., Secretst, J., Du, Z., Zheng, J.,
674 Shang, D., Zeng, L., Shao, M., Wang, W., Huang, Y., Wang, Y., Zhu, Y., Li, Y., Hu, J.,
675 Pan, B., Cai, L., Cheng, Y., Ji, Y., Zhang, F., Rosenfeld, D., Liss, P. S., Duce, R. A., Kolb,
676 C. E., and Molina, M. J.: Persistent sulfate formation from London Fog to Chinese haze,
677 *Proc Natl Acad Sci U S A*, 113, 13630-13635, 10.1073/pnas.1616540113, 2016a.

678 Wang, G., Zhang, R., Gomez, M. E., Yang, L., Zamora, M. L., Hu, M., Lin, Y., Peng, J.,
679 Guo, S., and Meng, J.: Persistent sulfate formation from London Fog to Chinese haze,
680 *Proceedings of the National Academy of Sciences*, 113, 13630-13635, 2016b.

681 Wang, H., Zhu, B., Zhang, Z., An, J., and Shen, L.: Mixing state of individual carbonaceous
682 particles during a severe haze episode in January 2013, Nanjing, China, *Particuology*, 20,
683 16-23, 10.1016/j.partic.2014.06.013, 2015.

684 Wang, H., Lu, K., Chen, X., Zhu, Q., Chen, Q., Guo, S., Jiang, M., Li, X., Shang, D., Tan,
685 Z., Wu, Y., Wu, Z., Zou, Q., Zheng, Y., Zeng, L., Zhu, T., Hu, M., and Zhang, Y.: High

686 N₂O₅ Concentrations Observed in Urban Beijing: Implications of a Large Nitrate
687 Formation Pathway, *Environ. Sci. Technol. Lett.*, 4, 416-420, 10.1021/acs.estlett.7b00341,
688 2017.

689 Wang, J., Liu, D., Ge, X., Wu, Y., Shen, F., Chen, M., Zhao, J., Xie, C., Wang, Q., Xu, W.,
690 Zhang, J., Hu, J., Allan, J., Joshi, R., Fu, P., Coe, H., and Sun, Y.: Characterization of black
691 carbon-containing fine particles in Beijing during wintertime, *Atmos. Chem. Phys.*, 19,
692 447-458, 10.5194/acp-19-447-2019, 2019.

693 Wang, P., Pan, B., Li, H., Huang, Y., Dong, X., Ai, F., Liu, L., Wu, M., and Xing, B.: The
694 Overlooked Occurrence of Environmentally Persistent Free Radicals in an Area with Low-
695 Rank Coal Burning, Xuanwei, China, *Environ. Sci. Technol.*, 52, 1054-1061,
696 10.1021/acs.est.7b05453, 2018.

697 Xie, C., Xu, W., Wang, J., Wang, Q., Liu, D., Tang, G., Chen, P., Du, W., Zhao, J., Zhang,
698 Y., Zhou, W., Han, T., Bian, Q., Li, J., Fu, P., Wang, Z., Ge, X., Allan, J., Coe, H., and
699 Sun, Y.: Vertical characterization of aerosol optical properties and brown carbon in winter
700 in urban Beijing, China, *Atmos. Chem. Phys.*, 19, 165-179, 10.5194/acp-19-165-2019,
701 2019.

702 Xu, J., Li, M., Shi, G., Wang, H., Ma, X., Wu, J., Shi, X., and Feng, Y.: Mass spectra
703 features of biomass burning boiler and coal burning boiler emitted particles by single
704 particle aerosol mass spectrometer, *Sci Total Environ*, 598, 341-352,
705 <https://doi.org/10.1016/j.scitotenv.2017.04.132>, 2017.

706 Xu, J., Wang, H., Li, X., Li, Y., Wen, J., Zhang, J., Shi, X., Li, M., Wang, W., Shi, G., and
707 Feng, Y.: Refined source apportionment of coal combustion sources by using single

708 particle mass spectrometry, *Sci. Total Environ.*, 627, 633-646,
709 10.1016/j.scitotenv.2018.01.269, 2018.

710 Xu, W. Q., Sun, Y. L., Chen, C., Du, W., Han, T. T., Wang, Q. Q., Fu, P. Q., Wang, Z. F.,
711 Zhao, X. J., Zhou, L. B., Ji, D. S., Wang, P. C., and Worsnop, D. R.: Aerosol composition,
712 oxidation properties, and sources in Beijing: results from the 2014 Asia-Pacific Economic
713 Cooperation summit study, *Atmos. Chem. Phys.*, 15, 13681-13698, 10.5194/acp-15-
714 13681-2015, 2015.

715 Zhai, J., Wang, X., Li, J., Xu, T., Chen, H., Yang, X., and Chen, J.: Thermal desorption
716 single particle mass spectrometry of ambient aerosol in Shanghai, *Atmos. Environ.*, 123,
717 407-414, 10.1016/j.atmosenv.2015.09.001, 2015.

718 Zhai, S., An, X., Zhao, T., Sun, Z., Hou, Q., and Wang, C.: Detecting critical
719 PM_{2.5} emission sources and their contributions to a heavy haze
720 episode in Beijing, China by using an adjoint model, *Atmospheric Chemistry and Physics
721 Discussions*, 2016, 1-20, 10.5194/acp-2016-911, 2016.

722 Zhang, R., Wang, G., Guo, S., Zamora, M. L., Ying, Q., Lin, Y., Wang, W., Hu, M., and
723 Wang, Y.: Formation of urban fine particulate matter, *Chem. Rev.*, 115, 3803-3855,
724 10.1021/acs.chemrev.5b00067, 2015.

725 Zhao, J., Qiu, Y., Zhou, W., Xu, W., Wang, J., Zhang, Y., Li, L., Xie, C., Wang, Q., Du,
726 W., Worsnop, D. R., Canagaratna, M. R., Zhou, L., Ge, X., Fu, P., Li, J., Wang, Z.,
727 Donahue, N. M., and Sun, Y.: Organic Aerosol Processing During Winter Severe Haze
728 Episodes in Beijing, *J. Geophys. Res. Atmos.*, 124, 10248-10263, 10.1029/2019JD030832,
729 2019.

730 Zheng, M., Yan, C. Q., Wang, S. X., He, K. B., and Zhang, Y. H.: Understanding PM2.5
731 sources in China: challenges and perspectives, *Natl Sci Rev*, 4, 801-803,
732 10.1093/nsr/nwx129, 2017.

733 Zou, Y., Deng, X. J., Zhu, D., Gong, D. C., Wang, H., Li, F., Tan, H. B., Deng, T., Mai, B.
734 R., Liu, X. T., and Wang, B. G.: Characteristics of 1 year of observational data of VOCs,
735 NO_x and O₃ at a
736 suburban site in Guangzhou, China, *Atmos Chem Phys*, 15, 6625-6636, 10.5194/acp-15-
737 6625-2015, 2015.

738